DOI: 10.1002/ange.201408533

Imaging of Bacteria

PET Imaging of Bacterial Infections with Fluorine-18-Labeled Maltohexaose**

Xinghai Ning, Wonewoo Seo, Seungjun Lee, Kiyoko Takemiya, Mohammad Rafi, Xuli Feng, Daiana Weiss, Xiaojian Wang, Larry Williams, Vernon M. Camp, Malveaux Eugene, W. Robert Taylor, Mark Goodman,* and Niren Murthy**

Abstract: *A positron emission tomography (PET) tracer composed of ^{18}F-labeled maltohexaose (MH^{18}F) can image bacteria in vivo with a sensitivity and specificity that are orders of magnitude higher than those of fluorodeoxyglucose (^{18}FDG). MH^{18}F can detect early-stage infections composed of as few as 10^5 E. coli colony-forming units (CFUs), and can identify drug resistance in bacteria in vivo. MH^{18}F has the potential to improve the diagnosis of bacterial infections given its unique combination of high specificity and sensitivity for bacteria.*

The diagnosis of bacterial infections remains a central challenge in medicine. Infections are currently diagnosed by culturing of tissue biopsies or blood samples.[1] However, these methods can only detect late-stage infections, which are challenging to treat. Bacterial infections therefore cause an enormous medical burden, for example, the mortality caused by bacterial infections was greater than the mortality caused by AIDS, breast cancer, and prostate cancer combined.[2] Bacterial infections can be treated effectively, if diagnosed and treated at an early stage, and if the presence of drug resistance is also established. However, this task is challenging at present because the symptoms of infections look identical to a variety of other illnesses, such as cancer and inflammation.[3] An imaging technology that can identify and localize bacterial infections with high sensitivity and specificity thus has the potential to have a significant impact on medicine in this clinical environment.

Positron emission tomography (PET) imaging has the potential to significantly improve the diagnosis of bacterial infections because of its unparalleled sensitivity.[4] However, ^{18}FDG is currently the only PET contrast agent available for clinical imaging of infections, and is problematic because it lacks specificity for bacteria and has a high uptake in mammalian cells.[5] ^{18}FDG therefore cannot distinguish bacterial infections from other pathologies such as cancer and inflammation, and cannot diagnose bacterial infections at an early stage.[5a,6] Although numerous experimental PET contrast agents have been developed for imaging bacterial infections, such as radiolabeled antibiotics,[7] antimicrobial peptides,[1a] antibodies,[8] or white blood cells,[9] these agents have had minimal clinical impact. Several factors have contributed to the lack of success of bacteria imaging agents, such as poor clearance as a result of nonspecific adsorption, low target-receptor expression on bacteria, or complicated radiochemical synthesis, which are challenging to perform in clinical radiochemistry labs.[10] Therefore, there is a great need for the development of new PET contrast agents that can image small numbers of bacteria with high specificity in vivo.[11]

Herein, we present a new PET tracer, composed of ^{18}F-labeled maltohexaose (MH^{18}F), that can image bacterial infections in vivo with unprecedented sensitivity and specificity (see Scheme 1). MH^{18}F targets the bacteria-specific maltodextrin transporter, which internalizes α-1,4-linked glucose oligomers (maltodextrins) as a source of glucose.[12] The maltodextrin transport system is an ideal target for imaging bacteria because of its high uptake of maltodextrins (K_m of 130 μM),[13] great specificity for bacteria, and the rapid clearance of maltodextrins from uninfected tissues.[14] In addition, the maltodextrin transporter is only functional in metabolically active bacteria and MH^{18}F uptake is therefore an indicator of bacterial viability,[14b,15] and potentially antibiotic efficacy. Finally, MH^{18}F should have minimal toxicity in humans because maltodextrins are a commonly used food additive.[16]

A synthetic strategy was devised to synthesize MH^{18}F through nucleophilic fluorination of the maltohexaose–brosylate precursor (**3**) with K^{18}F in the presence of kryptofix

[*] Dr. X. Ning,[+] Dr. S. Lee, Dr. M. Rafi, Dr. X. Feng, Dr. X. Wang, Prof. N. Murthy
Department of Bioengineering, UC Berkeley
284 Hearst Memorial Mining Building
UC Berkeley, Berkeley, CA 94720 (USA)
E-mail: nmurthy@berkeley.edu
Dr. W. Seo,[+] L. Williams, V. M. Camp, M. Eugene, Prof. M. Goodman
Department of Radiology and Imaging Sciences
Emory University (USA)
E-mail: mgoodma@emory.edu
Dr. K. Takemiya, Dr. D. Weiss
Division of Cardiology, Department of Medicine
Emory University School of Medicine (USA)
Prof. W. R. Taylor
Division of Cardiology, Department of Medicine and the Department of Biomedical Engineering, Emory University School of Medicine and the Atlanta VA Medical Center (USA)
E-mail: w.robert.taylor@emory.edu
[+] These authors contributed equally to this work.

[**] This project has been funded in part with Federal funds from the National Heart, Lung, and Blood Institute, National Institutes of Health, Department of Health and Human Services, under Contract No. NIH R01 1R01HL096796-02 (N.M.), NIH U01 268201000043C-0-0-1, NIH R211R21AI098799-01 (N.M.), NIH 7UM1AI068636-07, and NIH R01 AI088023-03.

Supporting information for this article is available on the WWW under http://dx.doi.org/10.1002/anie.201408533.

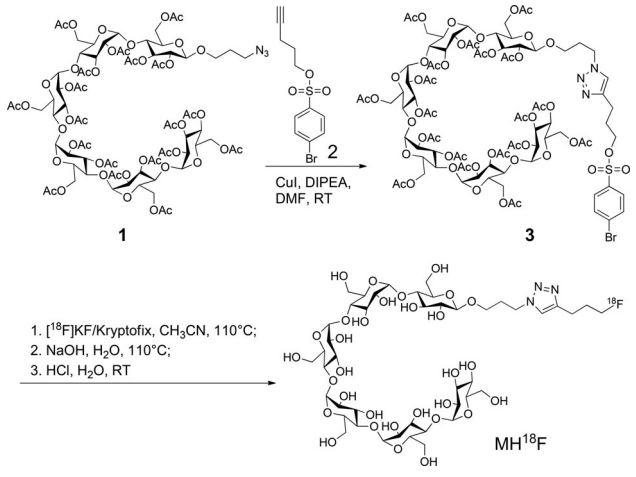

Scheme 1. Synthesis of $MH^{18}F$. $MH^{18}F$ is composed of ^{18}F-fluoride-conjugated to maltohexaose and was synthesized by a one-step nucleophilic ^{18}F fluorination of brosylate–maltohexaose (**3**).

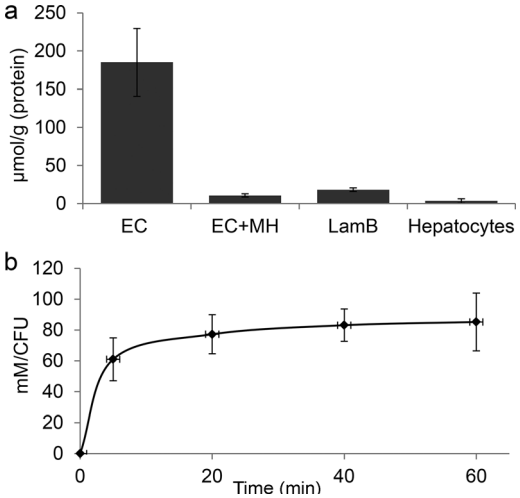

Figure 1. High specificity of $MH^{19}F$ for bacteria and robust internalization by bacteria. a) Specificity of $MH^{19}F$ for bacteria over hepatocytes. *E. coli* (EC), EC with LamB mutation (LamB), and mammalian cells were incubated with $MH^{19}F$ (500 μM) for 1 hour in the presence or absence of maltohexaose (MH; 50 mM). The intracellular $MH^{19}F$ concentration was determined and normalized to the protein content. Bacteria robustly accumulate $MH^{19}F$, whereas hepatocytes have negligible uptake. The uptake of $MH^{19}F$ in EC is inhibited by a large excess of maltohexaose, and the uptake of $MH^{19}F$ in LamB mutants is significantly reduced. The results are expressed as mean micromoles per gram of protein ± s.e.m. for $n = 3$ per group. b) Accumulation of $MH^{19}F$ in EC reaching millimolar concentrations. EC were incubated with $MH^{19}F$ (500 μM), and the intracellular concentration of $MH^{19}F$ was determined at different time points, $n = 3$ per group. s.e.m. = standard error of the mean.

k222 (see Scheme 1). The reducing end of maltohexaose was selected for the fluorination because the maltodextrin transporter recognizes the nonreducing end of maltodextrins and should therefore tolerate substitutions at the reducing end.[13a,17] Azide-functionalized maltohexaose **1** was synthesized from maltohexaose in four steps following established methods,[14b] and was conjugated with pent-4-yn-1-yl 4-bromobenzenesulfonate (**2**) using the Cu^{I}-catalyzed Huisgen cycloaddition to afford the brosylate–maltohexaose precursor (**3**).[18] Radiochemical synthesis of $MH^{18}F$ was carried out by cryptate-mediated nucleophilic substitution of the brosylate precursor **3** with potassium [^{18}F]fluoride ($K^{18}F$), followed by basic hydrolysis with NaOH and acid neutralization. A decay-corrected yield of 4.2% was obtained for this synthetic procedure, starting from ^{18}F-fluoride, with an 87% radiochemical purity based on radiometric HPLC (see Figure S5 in the Supporting Information).[19] The protocol for the preparation of $MH^{18}F$ had a synthesis time of 100 minutes and follows the same procedures used to prepare ^{18}FDG,[20] and should therefore be achievable in clinical radiochemistry laboratories. In addition, we anticipate that the radiochemical yield of $MH^{18}F$ can be increased using new ^{18}F-fluorination methodologies.[19]

$MH^{18}F$ is designed to selectively target bacteria because of the presence of maltodextrin transporters in bacteria, and their absence in mammalian cells. We therefore investigated if $MH^{19}F$ has specificity for bacteria over mammalian cells, and if it is internalized by the maltodextrin transporter LamB, using ^{19}F NMR spectroscopy. Bacteria (*E. coli)* and mammalian cells (hepatocytes) were incubated for one hour with $MH^{19}F$ at a concentration of 500 μM, washed with PBS, lysed, and the cellular supernatant was analyzed using ^{19}F NMR spectroscopy. Figure 1 a and 1 b demonstrate that $MH^{19}F$ has high specificity for bacteria over mammalian cells and is robustly internalized. For example, under these conditions, *E. coli* had accumulated two times more $MH^{19}F$ than hepatocytes, and reached intracellular concentrations in the millimolar range. In addition, we performed maltohexaose competition experiments and experiments with LamB mutant *E. coli* to determine if $MH^{19}F$ was internalized through the maltodextrin transport pathway. Figure 1 a demonstrates that the uptake of $MH^{19}F$ in *E. coli* could be inhibited by an excess of maltohexaose, and that there is minimal uptake of $MH^{19}F$ in LamB mutants, demonstrating that $MH^{19}F$ enters *E. coli* through the maltodextrin transport pathway.

We investigated the ability of $MH^{18}F$ to image bacterial infections in rats. *E. coli* (10^7 colony-forming units, CFUs) were injected into the left triceps muscle of rats, and the right triceps muscle was injected with PBS as a control. Two hours later, the rats were injected with 250 μCi of $MH^{18}F$ through the tail vein, and dynamic PET scans were performed using an Inveon micro PET/CT preclinical scanner (Siemens). Figure 2 a and b demonstrates that $MH^{18}F$ clears well from healthy tissue but is retained in infected muscle. For example, bacterial infections were clearly visible as early as 10 minutes after the injection with $MH^{18}F$ and had a high target-to-control contrast of 8.5 after 70 minutes, allowing bacterial infections to be easily visualized in vivo.

A key challenge in imaging bacteria is the development of probes that have high sensitivity for bacteria.[21] Current PET tracers for imaging bacteria, such as ^{18}FDG and radiolabeled antibiotics and antibodies, can only image 10^7–10^9 bacterial CFUs in vivo, and cannot detect infections at an early stage.[22] $MH^{18}F$ has the potential to detect small numbers of bacteria because of its fast transport into bacteria and its rapid clearance from uninfected tissues. We investigated the ability of $MH^{18}F$ to image early-stage bacterial infections. *E. coli* (10^5 CFUs) were injected into the left triceps muscle of rats and

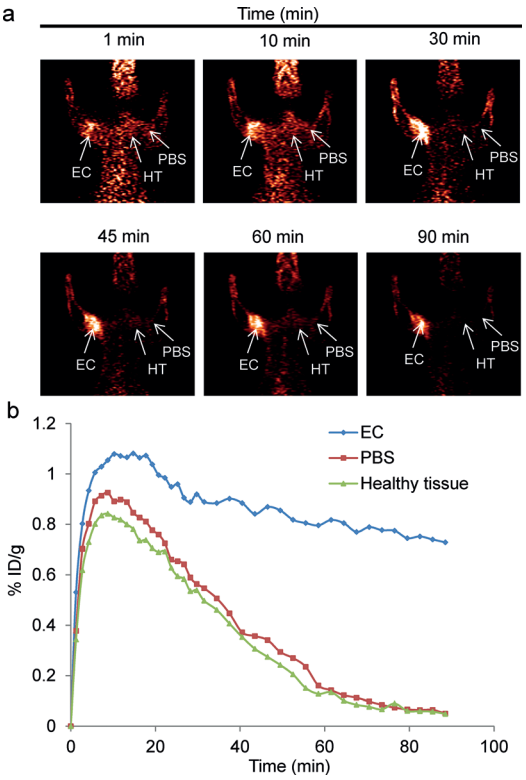

Figure 2. In vivo PET imaging of rats infected with *E. coli* (10^7 CFUs). a) Rats were infected in the left triceps muscle with 10^7 *E. coli,* administered with MH^{18}F, and dynamic PET scans were performed for 90 min using a microPET/CT. Infected muscles can be easily visualized after 90 min. b) Time activity curves of decay-corrected MH^{18}F activity in the infected rat, generated from Figure 2a. Infected muscle has an 8.5-fold increase in radioactivity over PBS-injected muscle. Arrows indicate the location of infected muscle (EC), PBS-injected muscle (PBS), and healthy tissue (HT). ID/g = % of injected dose/gram of tissue.

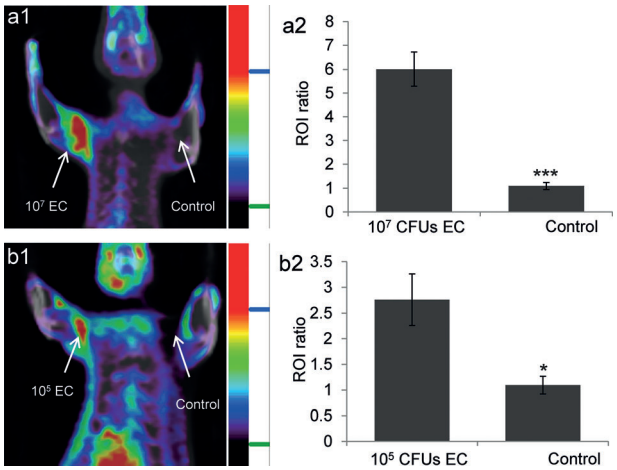

Figure 3. MH^{18}F can detect as few as 10^5 CFUs of *E. coli* (EC) in muscle infections. a1) MH^{18}F can detect 10^7 *E. coli* CFUs in rats. Rats were infected with 10^7 *E. coli* and imaged with MH^{18}F using a microPET/CT. The image of the rat is representative of four experiments, and identifies the infection site. a2) MH^{18}F generates a 6-fold increase in radioactivity in infected muscles. b1) MH^{18}F can detect as few as 10^5 *E. coli* in rats. Rats were infected with 10^5 *E. coli* CFUs and imaged with MH^{18}F using a microPET/CT. The image of the rat is representative of four experiments, and identifies the infection site. b2) MH^{18}F generates a 2.7-fold increase in radioactivity in infected muscles. Regions of interest (ROIs), including the infected muscles (target) or PBS injection areas (control) and healthy tissues (background), were identified and integrated using the ASI Pro VM micro PET analysis software. The results in a2 and b2 are expressed as the target or control to background ratio (ROI ratio) ± s.e.m. for $n = 4$ per group. The ROI ratio is defined as the mean radioactivity in the target/mean radioactivity in the background. The statistical significances in a2 and b2 were determined using a two-sample Student's *t*-test ($*p \le 0.05$ and $***p \le 0.001$).

imaged with MH^{18}F as described above. Figure 3b demonstrates that MH^{18}F is capable of detecting as few as 10^5 bacterial CFUs in vivo, for example, rat triceps muscles infected with 10^5 bacterial CFUs had a 2.7-fold increase in radioactivity over uninfected controls. Thus, the unique combination of robust transport into bacteria and clearance from healthy tissues allows MH^{18}F to image bacteria with high sensitivity.

^{18}FDG is currently the only PET radiopharmaceutical available for imaging bacterial infections; however, ^{18}FDG has significant limitations as a result of its high uptake in mammalian cells.[23] To determine the translational potential of MH^{18}F, a biodistribution study was performed with MH^{18}F and ^{18}FDG to compare their specificity for bacteria and nonspecific adsorption in healthy tissues. Rats were infected with 10^9 CFUs of *E. coli* and intravenously injected with either MH^{18}F or ^{18}FDG. One hour after the administration, various organs were harvested and their radioactivity was measured. Figure 4 demonstrates that MH^{18}F is specific for bacteria and has excellent clearance from healthy tissues. For example, MH^{18}F generated a 30-fold difference in accumulation between infected versus healthy muscles, and in contrast, ^{18}FDG generated only a 1.5-fold difference. The improved biodistribution pattern of MH^{18}F over ^{18}FDG is due to the

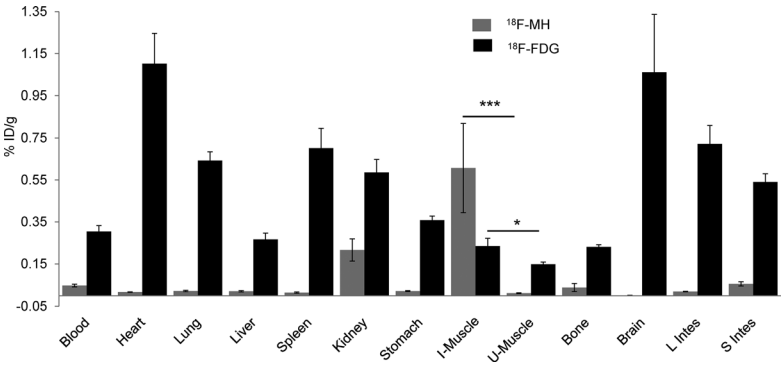

Figure 4. MH^{18}F is more effective than ^{18}FDG at imaging bacterial infections. A biodistribution study was performed with either MH^{18}F or ^{18}FDG in rats infected with 10^9 *E. coli* CFUs. MH^{18}F is efficiently cleared from uninfected tissues, whereas ^{18}FDG has significant accumulation within the major organs. The results are expressed as (% of injected dose)/(gram of tissue) ± s.e.m. for $n = 4$ per group. Statistical significance was determined using a two-sample Student's *t*-test ($*p \le 0.05$ and $***p \le 0.001$).

exclusive expression of maltohexaose transporters in bacteria in contrast to the high expression of glucose transporters in mammalian cells.[12c,24] This allowed MH^{18}F to clear from all of the major organs including heart, lung, brain, liver, bone, and muscle, whereas ^{18}FDG had significant accumulation within these tissues. For example, in infected rats, the ratio of accumulation of MH^{18}F in infected muscle versus liver was 5:1, whereas for ^{18}FDG, this ratio was only 0.3:1, and for other reported PET contrast agents the infected muscle to liver ratio is also generally less than 1:1.[1a,7–8] The excellent clearance of MH^{18}F allowed it to target bacteria much better than ^{18}FDG, and MH^{18}F therefore has the potential to image bacterial infections in a variety of anatomical areas.

At present, there is no direct method available to monitor the efficacy of antibiotic treatment, and doctors therefore have to rely on nonspecific and imprecise clinical indicators to guide antibiotic therapy.[25] MH^{18}F has the potential to image bacterial drug resistance because it targets ATP-binding cassette (ABC) transporters,[26] which require ATP for internalizing their substrates, connecting the uptake of MH^{18}F with cellular metabolism and bacterial viability. We therefore investigated if MH^{18}F could distinguish between live versus dead bacteria and identify resistance to therapy. We first performed PET imaging with MH^{18}F and ^{18}FDG, and compared their ability to monitor bacterial metabolic activity in vivo. Rats were injected with 10^9 CFUs of live *E. coli* in their left triceps and 10^9 CFUs of metabolically inactive *E. coli* (sodium azide treated) in their right triceps. Two hours later, the rats were injected with 250 μCi of either MH^{18}F or ^{18}FDG through the tail vein, and imaged using an Inveon micro PET/CT scanner. Figure 5a shows that MH^{18}F can distinguish between live versus metabolically inactive bacteria, for example metabolically active *E. coli* showed a 7-fold increase in relative radioactivity over metabolically inactive bacteria treated with sodium azide, demonstrating that MH^{18}F is actively transported by bacteria in vivo. In contrast, Figure 5b shows that ^{18}FDG could not distinguish between live versus dead bacteria because of its high uptake by inflammatory cells.

Based on these results, we investigated if MH^{18}F could identify bacterial drug resistance in vivo and measure antibiotic efficacy. Rats were infected with ampicillin-resistant *E. coli* (10^9 CFUs) and wild-type *E. coli* (10^9 CFUs), treated with ampicillin and imaged with MH^{18}F. Figure 6a demonstrates that MH^{18}F can measure the efficacy of antibiotics in vivo and rapidly identify drug resistance. For example,

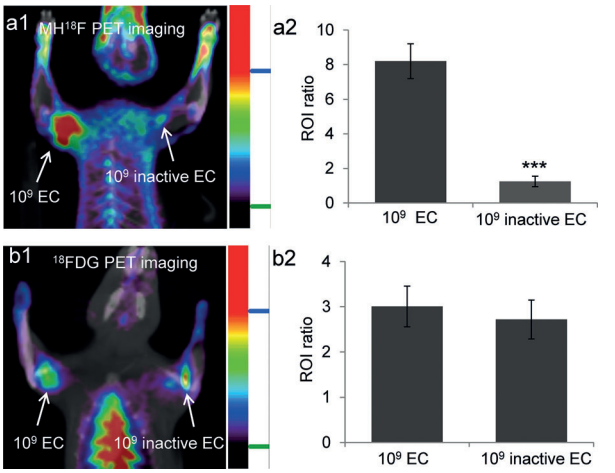

Figure 5. MH^{18}F can distinguish between live versus dead bacteria and can discriminate infections from inflammation. a1) MH^{18}F can distinguish between live versus dead bacteria in vivo. Rats were infected with 10^9 live and dead *E. coli* and imaged with MH^{18}F using a microPET/CT. The image of the rat is a representative result of four experiments and demonstrates that MH^{18}F does not accumulate in dead bacteria. a2) *E. coli* infected tissues had a 7-fold increase in radioactivity over muscles treated with dead bacteria. b1) ^{18}FDG cannot distinguish between live and dead *E. coli* infected tissues. Rats were infected with 10^9 live and dead *E. coli* CFUs and imaged with ^{18}FDG using a microPET/CT. The image is a representative result of four experiments and demonstrates that ^{18}FDG cannot discriminate live bacteria from dead bacteria. b2) ^{18}FDG accumulates in tissues infected with both live and dead bacteria. ROIs including the infected muscles (target) and healthy tissues (background) from a1 and b1 were identified and integrated using ASI Pro VM™ micro PET analysis software. The results in a2 and b2 are expressed as ROI ratio ± s.e.m. for $n = 4$ per group. The ROI ratio is defined as the mean radioactivity in the target/the mean radioactivity in the background. The statistical significance in a2 was determined using a two-sample Student's *t*-test (***$p \leq 0.001$).

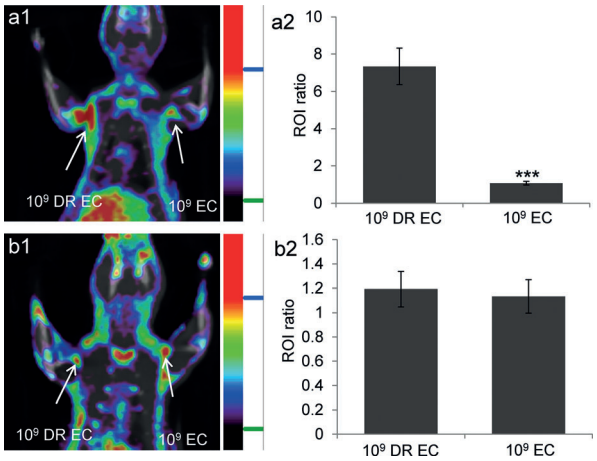

Figure 6. MH^{18}F can measure drug resistance and monitor the therapeutic effect of antibiotics in vivo. a1) MH^{18}F can identify drug resistance in bacteria in vivo. Rats were infected with 10^9 CFUs of ampicillin-resistant *E. coli* (DR EC) and wild-type *E. coli* (EC), treated with ampicillin and imaged with MH^{18}F using a microPET/CT. The image of the rat is representative of four experiments, and demonstrates that MH^{18}F only accumulates in DR EC infected muscles. a2) DR EC generated a 10-fold increase in radioactivity over EC. b1) MH^{18}F can monitor the therapeutic effect of antibiotics. Rats were infected with DR EC and EC, treated with ciprofloxacin and imaged with MH^{18}F using a microPET/CT. The image of the rat is representative of four experiments, and demonstrates that both DR EC and EC infected muscles have weak accumulation of MH^{18}F. a2) Both infected tissues have weak radioactivity. ROIs including the infected muscles (target) and healthy tissues (background) from a1 and b1 were identified and integrated using ASI Pro VM™ micro PET analysis software. The results in a2 and b2 are expressed as ROI ratio ± s.e.m. for $n = 4$ per group. The ROI ratio is defined as the mean radioactivity in the target/the mean radioactivity in the background. The statistical significance in a2 was determined using a two-sample Student's *t*-test (***$p \leq 0.001$).

ampicillin-resistant *E. coli* generated an 8.2-fold increase in PET signal intensity over susceptible *E. coli* because of their increased survival under antibiotic treatment. In addition, we investigated if $MH^{18}F$ could monitor the treatment of ampicillin-resistant bacteria with ciprofloxacin, and be used as a real-time methodology to assess antibiotic efficacy. Figure 6b demonstrates that in rats treated with ciprofloxacin, both tissues infected with ampicillin-resistant *E. coli* (10^9 CFUs) and wild-type *E. coli* (10^9 CFUs) have very low accumulation of $MH^{18}F$, indicating that $MH^{18}F$ can quantify the effects of antibiotics, and can be used to guide the selection of antibiotics.

In conclusion, we have presented a bacteria-targeted PET tracer, termed $MH^{18}F$, which can image bacteria in vivo with a sensitivity and specificity that are orders of magnitude higher than those of previously reported PET tracers. $MH^{18}F$ can also identify drug resistance and can therefore potentially assist physicians in prescribing the effective antibiotics. Finally, $MH^{18}F$ can be synthesized in one radiochemical step from clinically available $K^{18}F$, and therefore has the potential to rapidly enter into clinical trials.

Received: August 25, 2014
Published online: October 21, 2014

Keywords: bacterial infections · maltodextrin transporters · maltohexaose · positron emission tomography · radiochemistry

[1] a) A. Lupetti, M. M. Welling, E. K. Pauwels, P. H. Nibbering, *Lancet Infect. Dis.* **2003**, *3*, 223 – 229; b) L. J. van Doorn, Y. Henskens, N. Nouhan, A. Verschuuren, R. Vreede, P. Herbink, G. Ponjee, K. van Krimpen, R. Blankenburg, J. Scherpenisse, W. Quint, *J. Clin. Microbiol.* **2000**, *38*, 13 – 17.

[2] Sepsis fact sheet, http://www.nigms.nih.gov/Education/Pages/factsheet_sepsis.aspx (2014).

[3] a) A. Gillissen, M. Paparoupa, *Clin. Respir. J.* **2014**, DOI: 10.1111/crj.12135; b) K. S. Sfanos, W. B. Isaacs, A. M. De Marzo, *Am. J. Clin. Exp. Urol.* **2013**, *1*, 3 – 11.

[4] a) M. E. Phelps, *Proc. Natl. Acad. Sci. USA* **2000**, *97*, 9226 – 9233; b) S. M. Ametamey, M. Honer, P. A. Schubiger, *Chem. Rev.* **2008**, *108*, 1501 – 1516.

[5] a) A. W. Glaudemans, A. Signore, *Eur. J. Nucl. Med. Mol. Imaging* **2010**, *37*, 1986 – 1991; b) P. A. Erba, F. Bandera, M. Sollini, C. Tascini, *J. Am. Coll. Cardiol.* **2012**, *60*, 1435 – 1436; author reply 1437; c) Z. Keidar, S. Nitecki, *Semin. Nucl. Med.* **2013**, *43*, 396 – 402; d) T. del Rosal, W. A. Goycochea, A. Mendez-Echevarria, M. Garcia-Fernandez de Villalta, F. Baquero-Artigao, M. Coronado, M. D. Marin, L. Albajara, *Eur. J. Pediatr.* **2013**, *172*, 1111 – 1115.

[6] a) F. H. M. Corstens, J. W. M. van der Meer, *Lancet* **1999**, *354*, 765 – 770; b) F. Gemmel, N. Dumarey, M. Welling, *Semin. Nucl. Med.* **2009**, *39*, 11 – 26; c) M. van Oosten, T. Schäfer, J. A. C. Gazendam, K. Ohlsen, E. Tsompanidou, M. C. de Goffau, H. J. M. Harmsen, L. M. A. Crane, E. Lim, K. P. Francis, L. Cheung, M. Olive, V. Ntziachristos, J. M. van Dijl, G. M. van Dam, *Nat. Commun.* **2013**, *4*, 2584.

[7] O. Langer, U. Muller, M. Brunner, M. Zeitlinger, C. Joukhadar, M. Mitterhauser, W. Wadsak, K. Kletter, M. Muller, *Eur. J. Nucl. Med. Mol. Imaging* **2004**, *31*, S447 – S447.

[8] a) M. Rusckowski, S. Gupta, G. Liu, S. Dou, D. J. Hnatowich, *J. Nucl. Med.* **2004**, *45*, 1201 – 1208; b) H. J. Rennen, J. Makarewicz, W. J. Oyen, P. Laverman, F. H. Corstens, O. C. Boerman, *Nucl. Med. Biol.* **2001**, *28*, 401 – 408.

[9] a) A. Bhattacharya, R. Kochhar, S. Sharma, P. Ray, N. Kalra, N. Khandelwal, B. R. Mittal, *J. Nucl. Med.* **2014**, *55*, 1267 – 1272; b) H. A. Jones, A. M. Peters, J. C. Clark, *Nucl. Med. Commun.* **2001**, *22*, 601 – 602.

[10] a) M. Petrik, H. Haas, M. Schrettl, A. Helbok, M. Blatzer, C. Decristoforo, *Nucl. Med. Biol.* **2012**, *39*, 361 – 369; b) O. Langer, M. Brunner, M. Zeitlinger, S. Ziegler, U. Müller, G. Dobrozemsky, E. Lackner, C. Joukhadar, M. Mitterhauser, W. Wadsak, E. Minar, R. Dudczak, K. Kletter, M. Müller, *Eur. J. Nucl. Med. Mol. Imaging* **2005**, *32*, 143 – 150; c) N. Petruzzi, N. Shanthly, M. Thakur, *Semin. Nucl. Med.* **2009**, *39*, 115 – 123; d) C. Lu, Q. Jiang, C. Tan, J. Tang, J. Zhang, *Molecules* **2012**, *17*, 8518 – 8532.

[11] A. Signore, S. J. Mather, G. Piaggio, G. Malviya, R. A. Dierckx, *Chem. Rev.* **2010**, *110*, 3112 – 3145.

[12] a) H. A. Shuman, *Ann. Microbiol.* **1982**, *133A*, 153 – 159; b) P. E. Klebba, *Res. Microbiol.* **2002**, *153*, 417 – 424; c) A. Charbit, *Front. Biosci.* **2003**, *8*, s265 – 274; d) S. Gopal, D. Berg, N. Hagen, E. M. Schriefer, R. Stoll, W. Goebel, J. Kreft, *PLoS One* **2010**, *5*, e10349; e) W. Boos, H. Shuman, *Microbiol. Mol. Biol. Rev.* **1998**, *62*, 204 – 229.

[13] a) R. Dippel, W. Boos, *J. Bacteriol.* **2005**, *187*, 8322 – 8331; b) S. Freundlieb, U. Ehmann, W. Boos, *J. Biol. Chem.* **1988**, *263*, 314 – 320.

[14] a) R. Reuss, J. Ludwig, R. Shirakashi, F. Ehrhart, H. Zimmermann, S. Schneider, M. M. Weber, U. Zimmermann, H. Schneider, V. L. Sukhorukov, *J. Membr. Biol.* **2004**, *200*, 67 – 81; b) X. Ning, S. Lee, Z. Wang, D. Kim, B. Stubblefield, E. Gilbert, N. Murthy, *Nat. Mater.* **2011**, *10*, 602 – 607.

[15] A. J. Sharff, L. E. Rodseth, J. C. Spurlino, F. A. Quiocho, *Biochemistry* **1992**, *31*, 10657 – 10663.

[16] R. Shepherd, A. Robertson, D. Ofman, *Food Hydrocolloids* **2000**, *14*, 281 – 286.

[17] S. Freundlieb, U. Ehmann, W. Boos, *J. Biol. Chem.* **1988**, *263*, 314 – 320.

[18] a) Q. Wang, T. R. Chan, R. Hilgraf, V. V. Fokin, K. B. Sharpless, M. G. Finn, *J. Am. Chem. Soc.* **2003**, *125*, 3192 – 3193; b) H. C. Kolb, M. G. Finn, K. B. Sharpless, *Angew. Chem. Int. Ed.* **2001**, *40*, 2004 – 2021; *Angew. Chem.* **2001**, *113*, 2056 – 2075.

[19] a) D. O'Hagan, C. Schaffrath, S. L. Cobb, J. T. Hamilton, C. D. Murphy, *Nature* **2002**, *416*, 279; b) D. W. Kim, Y. S. Choe, D. Y. Chi, *Nucl. Med. Biol.* **2003**, *30*, 345 – 350; c) D. W. Kim, D. Y. Chi, *Angew. Chem. Int. Ed.* **2004**, *43*, 483 – 485; *Angew. Chem.* **2004**, *116*, 489 – 491; d) D. W. Kim, D. S. Ahn, Y. H. Oh, S. Lee, H. S. Kil, S. J. Oh, S. J. Lee, J. S. Kim, J. S. Ryu, D. H. Moon, D. Y. Chi, *J. Am. Chem. Soc.* **2006**, *128*, 16394 – 16397; e) M. Glaser, E. Arstad, *Bioconjugate Chem.* **2007**, *18*, 989 – 993; f) G. Vaidyanathan, M. R. Zalutsky, *Nucl. Med. Biol.* **1992**, *19*, 275 – 281; g) R. Iwata, C. Pascali, A. Bogni, G. Horvath, Z. Kovacs, K. Yanai, T. Ido, *Appl. Radiat. Isot.* **2000**, *52*, 87 – 92; h) O. Prante, J. Einsiedel, R. Haubner, P. Gmeiner, H. J. Wester, T. Kuwert, S. Maschauer, *Bioconjugate Chem.* **2007**, *18*, 254 – 262; i) R. Ting, M. J. Adam, T. J. Ruth, D. M. Perrin, *J. Am. Chem. Soc.* **2005**, *127*, 13094 – 13095; j) E. Lee, A. S. Kamlet, D. C. Powers, C. N. Neumann, G. B. Boursalian, T. Furuya, D. C. Choi, J. M. Hooker, T. Ritter, *Science* **2011**, *334*, 639 – 642; k) E. Lee, J. M. Hooker, T. Ritter, *J. Am. Chem. Soc.* **2012**, *134*, 17456 – 17458; l) M. Huiban, M. Tredwell, S. Mizuta, Z. Wan, X. Zhang, T. L. Collier, V. Gouverneur, J. Passchier, *Nat. Chem.* **2013**, *5*, 941 – 944.

[20] a) D. S. Surasi, P. Bhambhvani, J. A. Baldwin, S. E. Almodovar, J. P. O'Malley, *J. Nucl. Med. Technol.* **2014**, *42*, 5 – 13; b) R. Nakao, T. Ito, M. Yamaguchi, K. Suzuki, *Nucl. Med. Biol.* **2008**, *35*, 239 – 244.

[21] a) C. Bettegowda, C. A. Foss, I. Cheong, Y. Wang, L. Diaz, N. Agrawal, J. Fox, J. Dick, L. H. Dang, S. Zhou, K. W. Kinzler, B. Vogelstein, M. G. Pomper, *Proc. Natl. Acad. Sci. USA* **2005**, *102*,

1145 – 1150; b) B. A. Smith, W. J. Akers, W. M. Leevy, A. J. Lampkins, S. Xiao, W. Wolter, M. A. Suckow, S. Achilefu, B. D. Smith, *J. Am. Chem. Soc.* **2010**, *132*, 67 – 69.

[22] a) D. Pellegrino, A. A. Bonab, S. C. Dragotakes, J. T. Pitman, G. Mariani, E. A. Carter, *J. Nucl. Med.* **2005**, *46*, 1522 – 1530; b) A. J. Fischman, E. Livni, J. Babich, N. M. Alpert, Y. Y. Liu, E. Thom, R. Cleeland, B. L. Prosser, R. J. Callahan, J. A. Correia, *Antimicrob. Agents Chemother.* **1992**, *36*, 2286 – 2292.

[23] a) L. Varagnolo, M. P. M. Stokkel, U. Mazzi, E. K. J. Pauwels, *Nucl. Med. Biol.* **2000**, *27*, 103 – 112; b) M. M. Hanasono, L. D. Kunda, G. M. Segall, G. H. Ku, D. J. Terris, *Laryngoscope* **1999**, *109*, 880 – 885; c) P. Lind, I. Igerc, T. Beyer, P. Reinprecht, K. Hausegger, *Eur. J. Nucl. Med. Mol. Imaging* **2004**, *31*, S125 – S134; d) N. Lubezky, U. Metser, R. Geva, R. Nakache, E. Shmueli, J. M. Klausner, E. Even-Sapir, A. Figer, M. Ben-Haim, *J. Gastrointest. Surg.* **2007**, *11*, 472 – 478.

[24] a) L. G. Strauss, D. Koczan, S. Klippel, L. Pan, S. Willis, C. Sachpekidis, A. Dimitrakopoulou-Strauss, *Am. J. Nucl. Med. Mol. Imaging* **2013**, *3*, 417 – 424; b) P. Deron, C. Vangestel, I. Goethals, A. De Potter, M. Peeters, H. Vermeersch, C. Van de Wiele, *Nuklearmedizin* **2011**, *50*, 15 – 21; c) C. Wandersman, *Ann. Microbiol.* **1982**, *133A*, 161 – 163.

[25] J. A. Roberts, R. Norris, D. L. Paterson, J. H. Martin, *Br. J. Clin. Pharmacol.* **2012**, *73*, 27 – 36.

[26] S. Morbach, S. Tebbe, E. Schneider, *J. Biol. Chem.* **1993**, *268*, 18617 – 18621.

